Journal of Power Sources 261 (2014) 93–100

Contents lists available at ScienceDirect

Journal of Power Sources

journal homepage: www.elsevier.com/locate/jpowsour

Porous $LiNi_{0.5}Mn_{1.5}O_4$ microspheres with different pore conditions: Preparation and application as cathode materials for lithium-ion batteries

Xiaobo Zhu [a], Xiaona Li [a], Youngchun Zhu [a,*], Shasha Jin [a], Yan Wang [a], Yitai Qian [a,b,*]

[a] Hefei National Laboratory for Physical Science at Microscale and Department of Chemistry, University of Science and Technology of China, Hefei, Anhui 230026, PR China
[b] Key Laboratory of Colloid and Interface Chemistry (Shandong University), Ministry of Education, and School of Chemistry and Chemical Engineering, Shandong University, Jinan 250100, PR China

HIGHLIGHTS

- Porous $LiNi_{0.5}Mn_{1.5}O_4$ microspheres are produced through a simple two-step method.
- The pore condition is able to be altered by changing the lithium sources.
- Microspheres with larger pores exhibit excellent rate and cycle performance.
- Tinier pores coupled with larger surface area show distinct disadvantages.

GRAPHICAL ABSTRACT

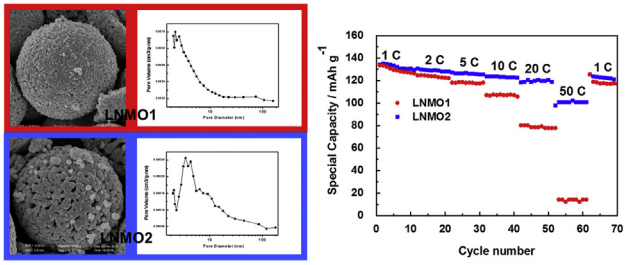

ARTICLE INFO

Article history:
Received 11 December 2013
Received in revised form
26 February 2014
Accepted 14 March 2014
Available online 21 March 2014

Keywords:
Lithium-ion batteries
High-voltage cathode materials
Lithium nickel manganese oxides
Porous microspheres
Pore condition

ABSTRACT

Here two types of $LiNi_{0.5}Mn_{1.5}O_4$ (LNMO) microspheres with different pore conditions are prepared through a facile two-step method. Initially, nickel manganese carbonate microspheres are obtained through a solvothermal reaction, and then they are heated with different lithium sources to obtain the two products. Scanning electron microscopy images clearly disclose that the two types of microspheres are respectively covered with dense tinier pores and sparse larger pores while both of their interiors are constituted by nanoparticles in similar size. Nitrogen adsorption/desorption analyses indicate that their maximum pore diameters are 2.2 nm and 3.5 nm. As cathodes of lithium ion batteries, the LNMO microspheres equipped with larger pores exhibit much more excellent electrochemical performance especially in terms of rate performance, achieving a discharge capacity of 101.7 mAh g^{-1} even at 50C, while their counterparts only receive 14.3 mAh g^{-1} coupled with severe polarization. And the capacities of them respectively maintain at 102.9 and 67 mAh g^{-1} after 100 cycles at 20C. Their distinct performance is suggested due to both the pore parameter and its related surface area.

1. Introduction

During the last decades, a wide range of transition metal oxides have been investigated and developed into electrode materials of lithium-ion batteries (LIBs). Among them, high-voltage $LiNi_{0.5}Mn_{1.5}O_4$ (LNMO), [1] as a derivative of spinel $LiMn_2O_4$, has

* Corresponding authors. Hefei National Laboratory for Physical Science at Microscale and Department of Chemistry, University of Science and Technology of China, Hefei, Anhui 230026, PR China.
E-mail addresses: ychzhu@ustc.edu.cn (Y. Zhu), ytqian@ustc.edu.cn (Y. Qian).

http://dx.doi.org/10.1016/j.jpowsour.2014.03.047
0378-7753/

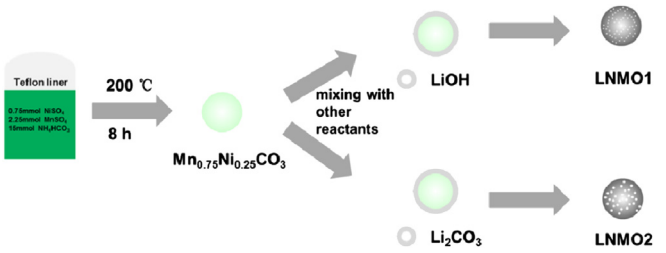

Scheme 1. Schematic illustration of the formation of two types of LNMO microspheres.

been considered as one of the hottest cathode candidates, which possess the advantages of considerably improved energy density, abundant raw materials and good stability. Generally, attributing to the theoretical capacity at 146.7 mAh g^{-1} and the high working voltage at 4.7 V, LNMO shows 20% and 30% higher energy density than conventional $LiCoO_2$ and $LiFePO_4$, respectively [2,3].

Apart from the inherent properties of the material, other attributes, including particle size, pore structure and morphology are also important and should be optimized [4]. Therefore, LNMO nanostructures with different morphologies, such as nanoparticle [5,6], nanorod [7], hierarchical micro-nano structure [8], porous nanorod [9], hollow microsphere or microcube [10], appear to be interesting, as they lead to improved kinetic performance by reducing the transport path lengths of lithium ions and electrons. However, some nanostructured materials with high surface area increase the incidence of undesirable electrode/electrolyte reactions [4]. Moreover, the situation may deteriorate in LNMO due to its high operation voltage, which nearly reaches the window of stability of the electrolyte solutions [11,12]. Porous micron materials, therefore, are reasonable to be designed in this case. Specifically, their relative high interfacial and continuous porous transport pores network, allowing for efficient ion transport thereby improving the rate capability of the LIBs [13]. Moreover, it has been established that microspheres, including $LiCoO_2$ [14],

Fig. 2. XRD patterns of the two products.

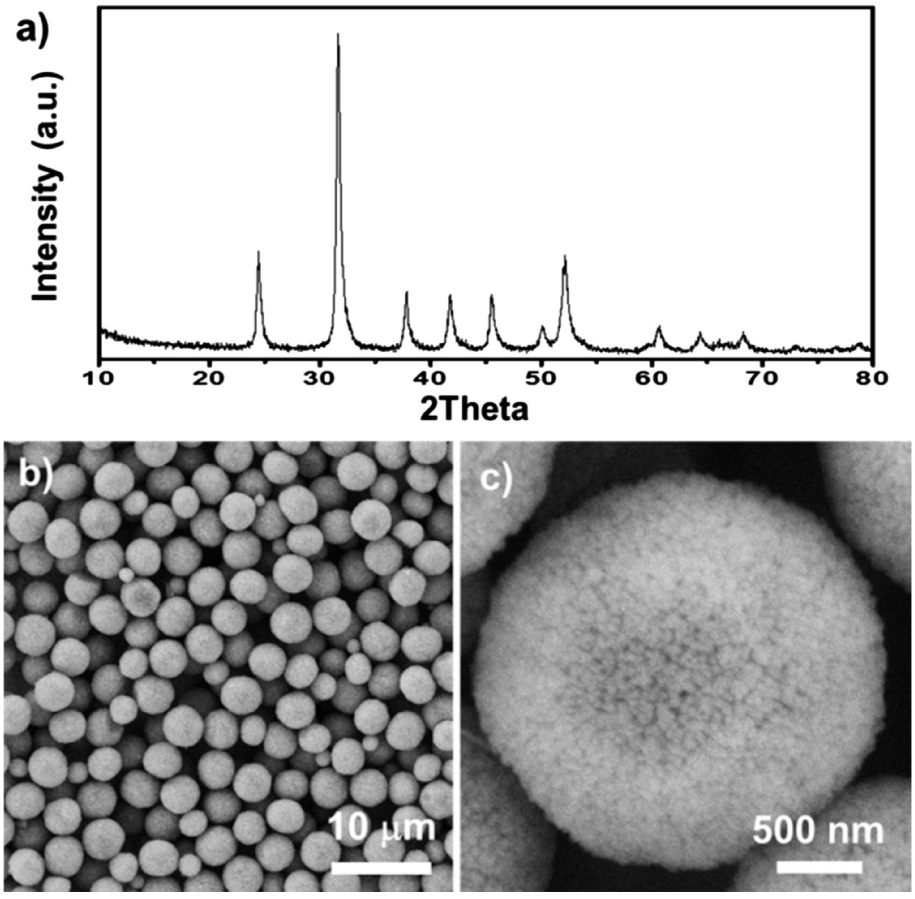

Fig. 1. XRD pattern (a) and SEM images under different magnifications (b, c) of $Mn_{0.75}Ni_{0.25}CO_3$.

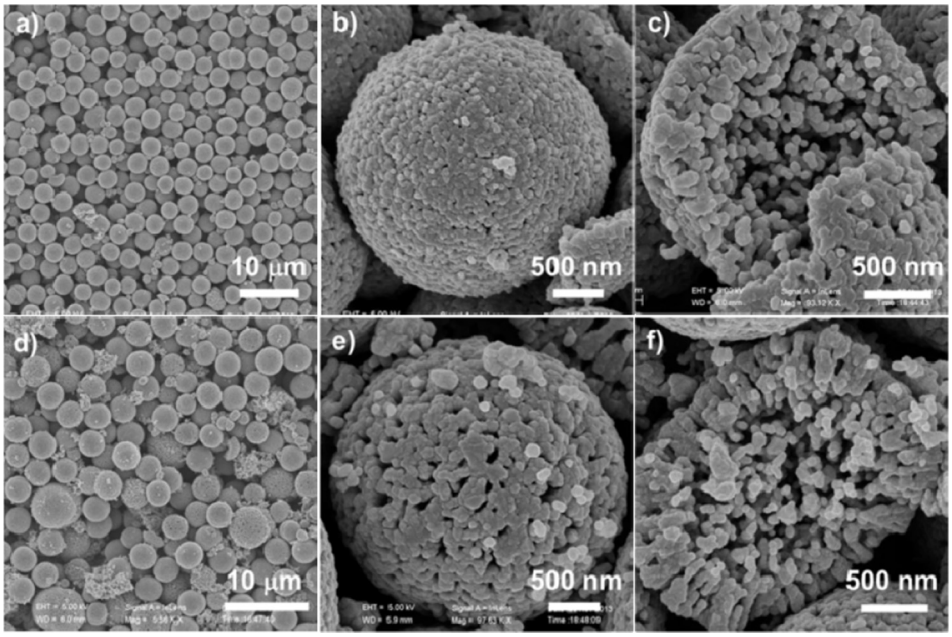

Fig. 3. SEM images under different magnifications of LNMO1 (a, b, c) and LNMO2 (d, e, f).

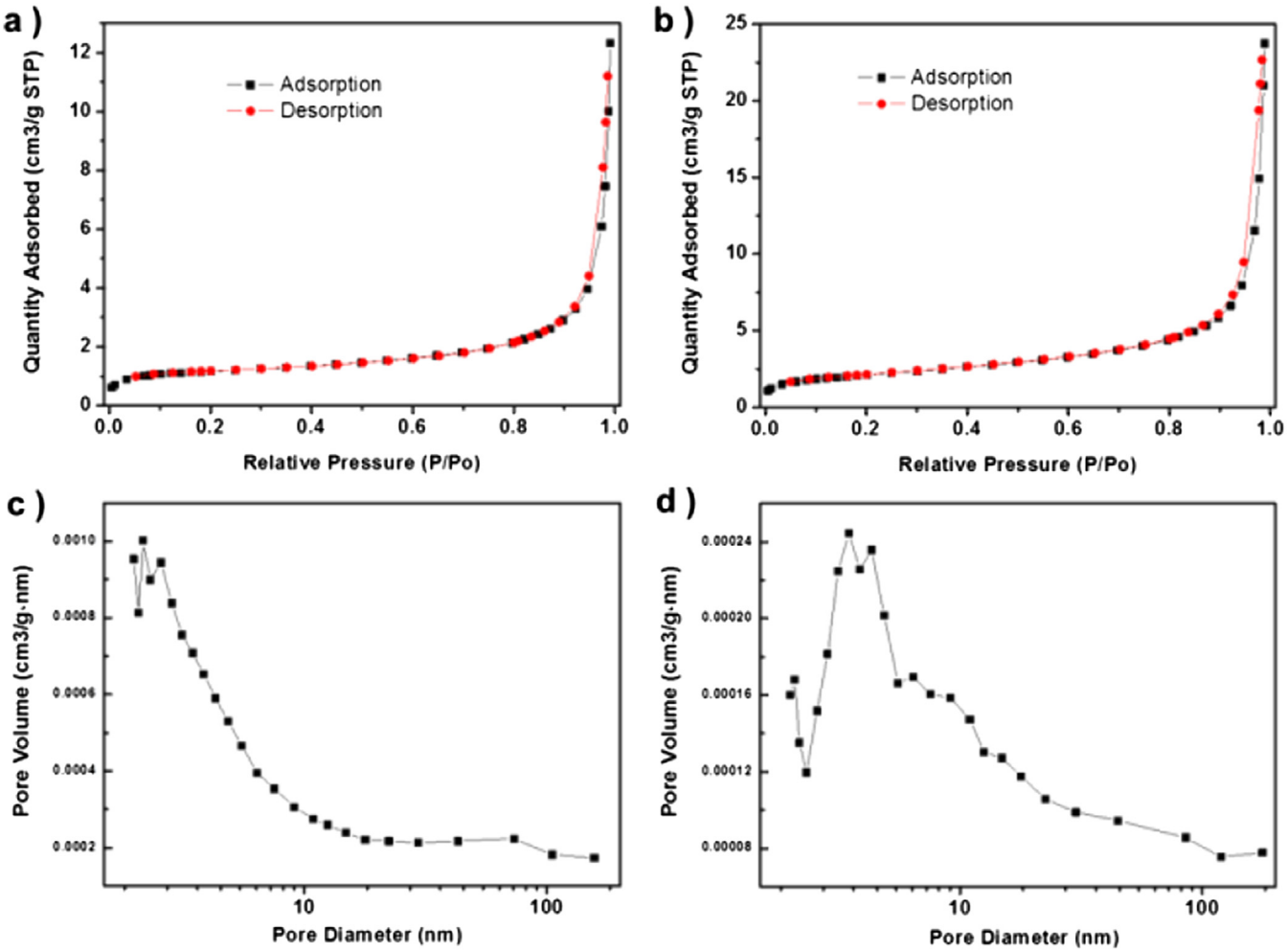

Fig. 4. The N_2 adsorption–desorption isotherm loop (a, b) and a histogram of the pore size distribution data (c, d) for the synthesized LNMO1 (a, c) and LNMO2 (b, d).

$LiMn_2O_4$ [15], $LiFePO_4$ [16], and $Li_4Ti_5O_{12}$ [17], allow packing efficiencies and high tap densities. Such efficient packing brings a high volumetric specific energy, which has important prospects in many practical and commercial applications, and a possibility of lowering the hazard caused by spurious reactions in LNMO as well.

Herein, we provide a facile design and a comparative study to two types of LNMO porous microspheres in terms of different pore size. As shown in Scheme 1, the preparation processes both start from the nickel manganese carbonate $Mn_{0.75}Ni_{0.25}CO_3$ microspheres, which are prepared through a solvothermal reaction. Then the $Mn_{0.75}Ni_{0.25}CO_3$ microspheres are directly blended and heated with two kinds of lithium sources, LiOH and Li_2CO_3, respectively. Their difference in pores distribution is clearly identified by scanning electron microscope and nitrogen adsorption/desorption analysis. Finally, the electrochemical properties of as-prepared two samples are investigated as cathode materials for LIBs thereby disclosing the influence of pore size of the LNMO microspheres to their electrochemical performance.

2. Experimental section

2.1. Synthesis of $Mn_{0.75}Ni_{0.25}CO_3$ microspheres

All the chemical reagents used here were analytical grade without further purification. In a typical synthesis process, $MnSO_4 \cdot H_2O$ (2.25 mmol) and $NiSO_4 \cdot 6H_2O$ (0.75 mmol) was dissolved in 30 mL mixed solvent (20 mL distill water and 10 mL ethanol) to form solution A, and 15 mmol NH_4HCO_3 was dissolved in 20 mL distill water to form solution B. Then solution B was added into solution A under stirring and continued to stir for 30 min. Afterward, the mixture was transferred to a 60 mL Teflon lined stainless-steel autoclave. The autoclave was sealed and maintained at 200 °C for 8 h in an electron oven. After that, the precipitates in the autoclave were collected and washed by distilled water and absolute ethanol several times. At last, the precursors were dried in vacuum oven for further treatment.

2.2. Synthesis of LNMO microspheres

In the successive step, $Mn_{0.75}Ni_{0.25}CO_3$ microspheres were respectively grinded with required amount of $LiOH \cdot H_2O$ and Li_2CO_3 (both with 4% Li excess) aided by small amount of ethanol until forming solid powders. Eventually, the two types of LNMO microspheres with different pore sizes were obtained by calcining the dry mixtures at 700 °C for 8 h, named LNMO1 and LNMO2.

2.3. Characterization

X-ray powder diffraction (XRD) pattern of the products were recorded on a Philips X'pert X-ray diffractometer with Cu Ka radiation ($k = 1.54182$ Å). The microstructure was observed on a field-emitting scanning electron microscope (SEM, JEOL-JSM-6700F) and a high-resolution transmission electron microscope (HRTEM, JEOL-2010) with an accelerating voltage of 200 kV. The N_2 adsorption/desorption tests were determined by Brunauer–Emmett–Teller (BET) measurements using a Micromeritics ASAP 2020 accelerated surface area and porosimetry system. The tap densities of materials were examined by BT-1000 Powder Comprehensive Performance (Dandong Baite Instrument Co., Ltd.).

2.4. Electrochemical measurements

Charge/discharge tests were carried out using coin-type cells (size: 2016), which consisted of an active material working electrode and a Li foil counter electrode separated by a Celgard 2300 microporous membrane. To prepare the working electrode, active material, super P carbon black, and polyvinylidene fluoride (PVDF) were mixed by the weight ratio of 75:20:5 with *N*-methyl pyrrolidone (NMP) serving as the solvent to obtain a slurry. After coating the slurry onto an aluminum mesh current collector, the electrode was dried at 120 °C in vacuum for 12 h. Typical loadings of the

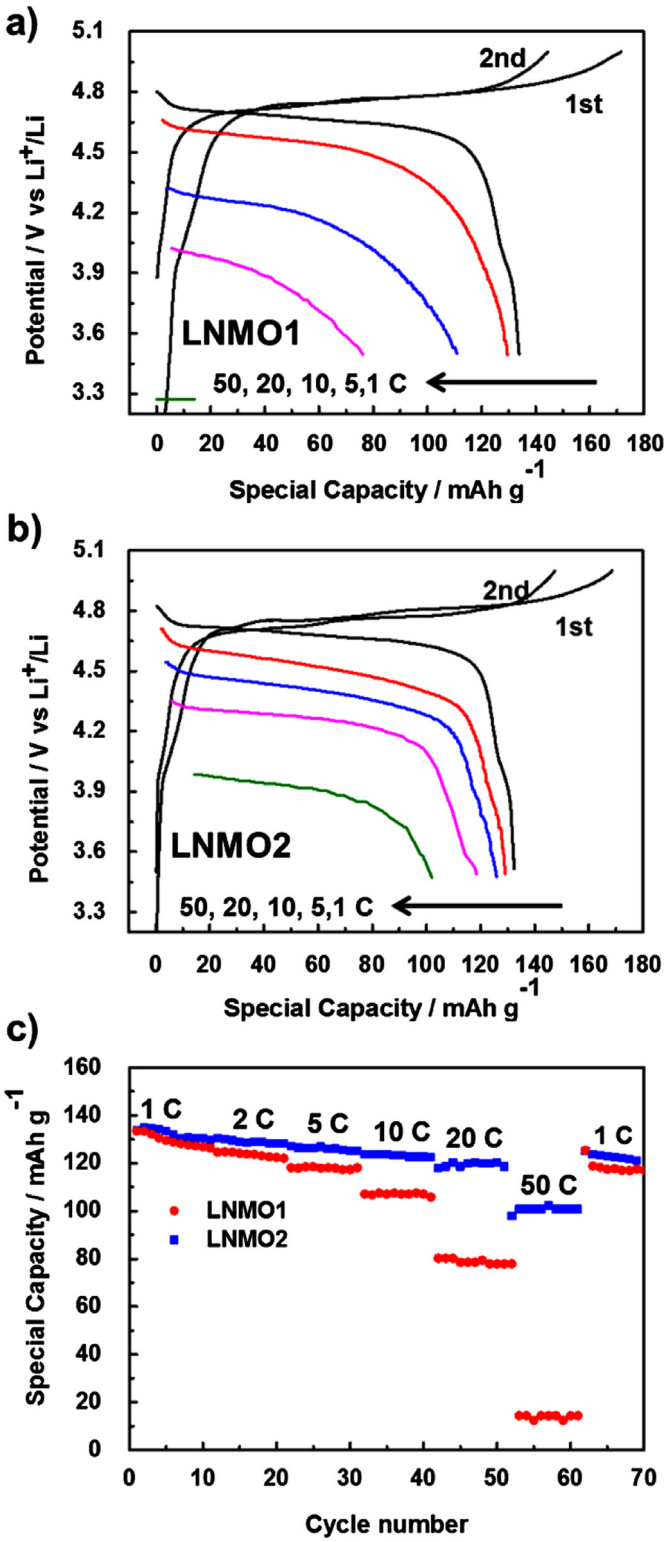

Fig. 5. Charge–discharge curves (a, b) and capacities (c) of the LNMO1, LNMO2 by discharge sequentially from 1C to 50C for per 10 cycles.

electrodes were between 1 and 2 mg of active material. 1 mol L^{-1} solution of $LiPF_6$ dissolved in ethylene carbonate/dimethyl carbonate (EC/DMC) (1:1 volume ratio) was used as the electrolyte. The cells were assembled in an argon-filled glove box (Mikrouna, Super 1220/750/900, China). The charge–discharge tests were performed on a LAND battery test system (LAND, CT2001A) in the range of 3.5–5.0 V (vs Li/Li^+) at different rates. The impedance spectroscopy (EIS) was recorded with an electrochemical workstation in a frequency range from 1 MHz to 0.01 Hz (Chenhua, Shanghai).

3. Results and discussion

Fig. 1a shows the typical XRD (X-ray powder diffraction) patterns of the $Mn_{0.75}Ni_{0.25}CO_3$ microspheres. Interestingly, separated $MnCO_3$ and $NiCO_3$ peaks cannot be detected. Fig. 1b shows the low-magnification scanning electron microscopy (SEM) image of $Mn_{0.75}Ni_{0.25}CO_3$ microspheres. According to the image, the carbonate precursors are basically in uniform spherical shape with a size around 3 μm. Moreover, the high-magnification image (Fig. 1c) focusing on a single microsphere reveals the microsphere is closely constituted by a host of nanoparticles, which lays a foundation for the subsequent products.

The XRD patterns of the two LNMO products are shown in Fig. 2. According to the two patterns, both of them possess the same sharp peaks indicating fine crystallinity and can be well indexed into a spinel phase (JCPDS card No. 80-2184 or 80-2162), only minor impurity peaks attributed to rock salt phase appear as conventional case [1]. Hence, the switch of two kinds of lithium sources hardly triggers any differences in their crystal structure.

Fig. 3 presents the SEM images of the two types of LNMO products. From the panoramic perspective (Fig. 3a, d), the two resultants display the spherical morphology with fine uniformity originated from the carbonate precursors. And the sizes of these microspheres approximately remain around 3 μm. Interestingly, high-magnification SEM images (Fig. 3b, e) focused on each typical single microsphere of the two products indicate they apparently differ from each other: dense and small pores are distributed on the surfaces of microspheres in LNMO1, in strong contrast, the external pores in LNMO2 are much larger and sparser. Besides, from the images of the broken spheres (Fig. 3c, f), their inner parts are similarly composed of numerous nanoparticles with same diameter about dozens of nanometers.

In order to gain further insight into the porous structure and pore size distribution of the two types of LNMO microspheres, Brunauer–Emmett–Teller (BET) measurements were conducted to examine their specific textural properties. As shown in Fig. 4a, b, the nitrogen adsorption–desorption isotherm can be attributed to type IV, according to IUPAC classification. And the hysteresis loops in the range of *ca.* $0.8–1.0P/P_0$, indicating the presence of mesopores possibly formed by the porous stacking of component

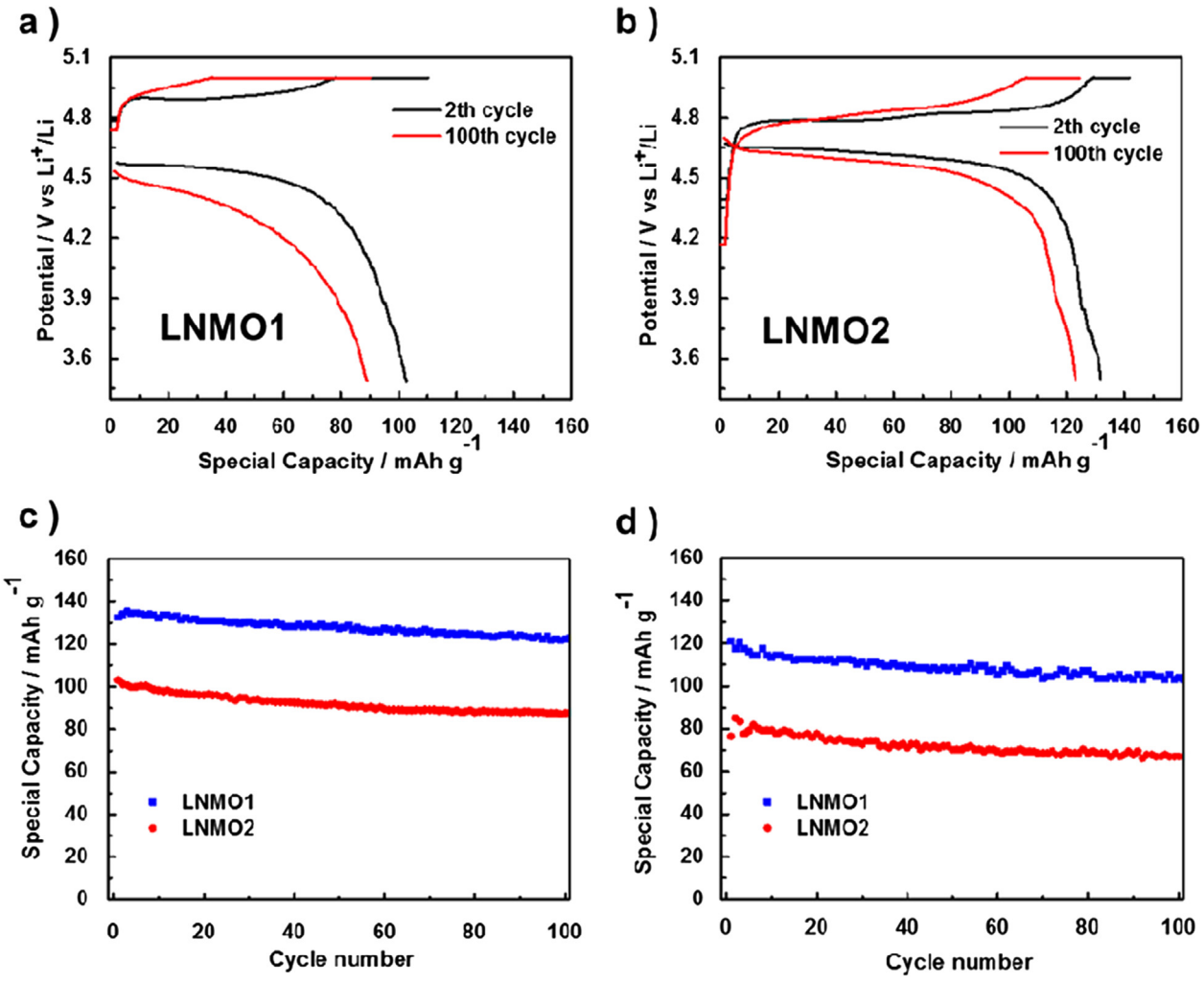

Fig. 6. Charge–discharge curves (a, b) of LNMO1 and LNMO2 at 10C. Cycling capacities of the two samples at 10C (c) and 20C (d) for 100 cycles.

nanoparticles [17]. The corresponding Barrett–Joyner–Halenda (BJH) pore size distribution curves (Fig. 4c–d) show that the sizes of pores involved in both of the microspheres are relatively concentrated, and an evident right shift of pore size from LNMO1 to LNMO2 can be observed. More exactly, their maximum pore diameters are 2.2 nm and 3.5 nm. Additionally, the BET measurements also disclose the surface areas of LNMO1 and LNMO2 amount to 7.54 and 4.06 $m^2\ g^{-1}$. And the BJH adsorption average pore diameter ($4V/A$) of them are 22.1 nm and 29.6 nm, separately, which are responsible for their difference in stacking of component nanoparticles.

Fig. 5 shows the discharge abilities of LNMO1 and LNMO2 at a series of rates from 1C to 50C (the charge rate is fixed at 1C). According to Fig. 5a, when charge and discharge rate is set at 1C, LNMO1 clearly displays the inherent merit of LNMO as an attractive cathode material based on the dominant charge and discharge plateaus around 4.7 V, which is attributed to the Ni^{2+}/Ni^{4+} redox couple. However, when the discharge rate ascends up, LNMO1 fails to maintain such advantage but falls into severe polarization and lower discharge capacities. In particular, its discharge potential range is below 4.05 V at 20C, and the capacity is shrunk to 80.2 mAh g^{-1}. And the situation is much negative when the discharge rate rising to 50C with onset potential at 3.3 V and negligible capacity about 14 mAh g^{-1}. In contrast, LNMO2 which possesses larger pores show substantially improved performance at higher rates in spite of their consistent electrochemical activity at 1C. Specifically, in accordance with Fig. 5b, when the discharge rate is respectively turned to 20 and 50C, discharge voltage plateau is started from 4.4 and 4.0 V together with much higher capacities amounting to 118.1 and 100.8 mAh g^{-1}, separately. Considering all the charge–discharge curves about the two samples, polarization is a determinant to the divergence of their electrochemical performance.

Towards better evaluation of their electrochemical properties, we also examine cycle performance of the two samples under constant charge and discharge at 10 and 20C, the constant rate charge step is followed by an additional constant voltage charge step till the current drops to 1C and 2C, respectively. The results are shown in Fig 6. Fig. 6a illustrates the 2nd and 100th charge–discharge profiles of LNMO1 at 10C. Evidently, the initial charge potential shoots up to nearly 4.8 V, and the proportion of capacity contributed by constant voltage charge experiences a huge rise as well. Therefore, serious polarization has again happened in LNMO1 and the constant voltage charge here plays a pivotal role in its capacity retention. Comparatively, as shown in Fig. 6b, the charge–discharge curves of LNMO2 possess good consistence over the 100 cycles at 10C, the initial charge potential is below 4.4 V and decreases to 4.2 V after cycles and the discharge potential starts from 4.7 V with a marginal variation over the 100 cycles. Correspondingly, only a small amount of capacity is ascribed to certain constant voltage charge process. All these constitute proofs of greatly alleviated polarization comparing with LNMO1. Fig. 6c–d shows the cycle performance of LNMO1 and LNMO2 at 10 and 20C. Both of them demonstrate good stability under rapid charge and discharge. Specifically, LNMO1 delivers 88 and 67 mAh g^{-1}, equivalent to 85% and 88% of its initial capacities at 10 and 20C, separately. Turn to LNMO2, the discharge capacities after 100 cycles at 10 and 20C are 122.8 and 102.9, which equate 93% and 85% capacity retention. Taking the degradation of discharge voltage of LNMO1 into consideration, its energy density retention is much worse than LNMO2.

In an effort to gain a better understanding of substantial difference of the performance of the two types of LNMO microspheres, the electrochemical impedance spectroscopy (EIS) of cells assembled with LNMO before cycle and after 1, 5 cycles at 1C were analyzed (Fig. 7). Base on the literature, [18,19] the starting point represents solution resistance (R_e). R_{sf} and CPE1 signify the diffusion resistance of Li^+ ions through the solid–electrolyte interface (SEI) layer and the corresponding constant phase element (CPE), R_{ct} and CPE2 correspond to the charge transfer resistance and the corresponding CPE and the slope of the line indicates the solid-state diffusion of Li^+ ions in the active materials (R_w). According to the spectra before cycle of the two samples, before cycle, both of them have a semicircle observed at the high frequency region and an oblique line at low frequency. And their R_e and R_w are mostly at similar level. As a result, without the formation of SEI layers, LNMO1 exhibits slightly lower charge transfer resistance, which can be explained by the larger surface area of tinier pores allowing better exposure of active materials to the electrolyte. After cycles, added semicircles appear the higher frequency range in both of the cells, attributing to SEI layers, which are also reflected in their higher charge capacities of first charge. Notably, in a significant shift, the R_{ct} and R_{sf} of LNMO2 are dramatically reduced, similar to other report [19]. In contrast, the resistances of LNMO1 are evidently increased, corresponding to its inferior rate performance. It is believed that the change of impedance has connection with the variation with the surface condition.

Further investigation of the surface conditions of the two samples after 5 cycles is carried out by the high-resolution TEM (HRTEM). Fig. 8b, d shows the magnified images of random corners of the two microspheres after several cycles at 1C. The amorphous layers with thickness of 1.5–2 nm are clearly observed on the

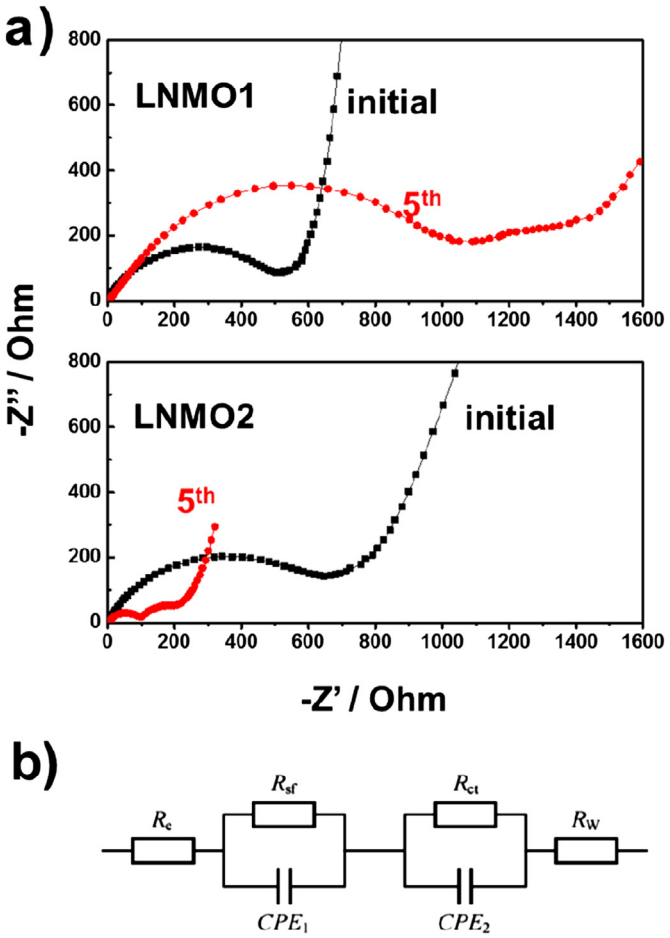

Fig. 7. EIS results of cells assembled with LNMO1 and LNMO2 (initial and 5th cycle) (a), the corresponding equivalent circuit. (b) Note that abbreviations defined in text.

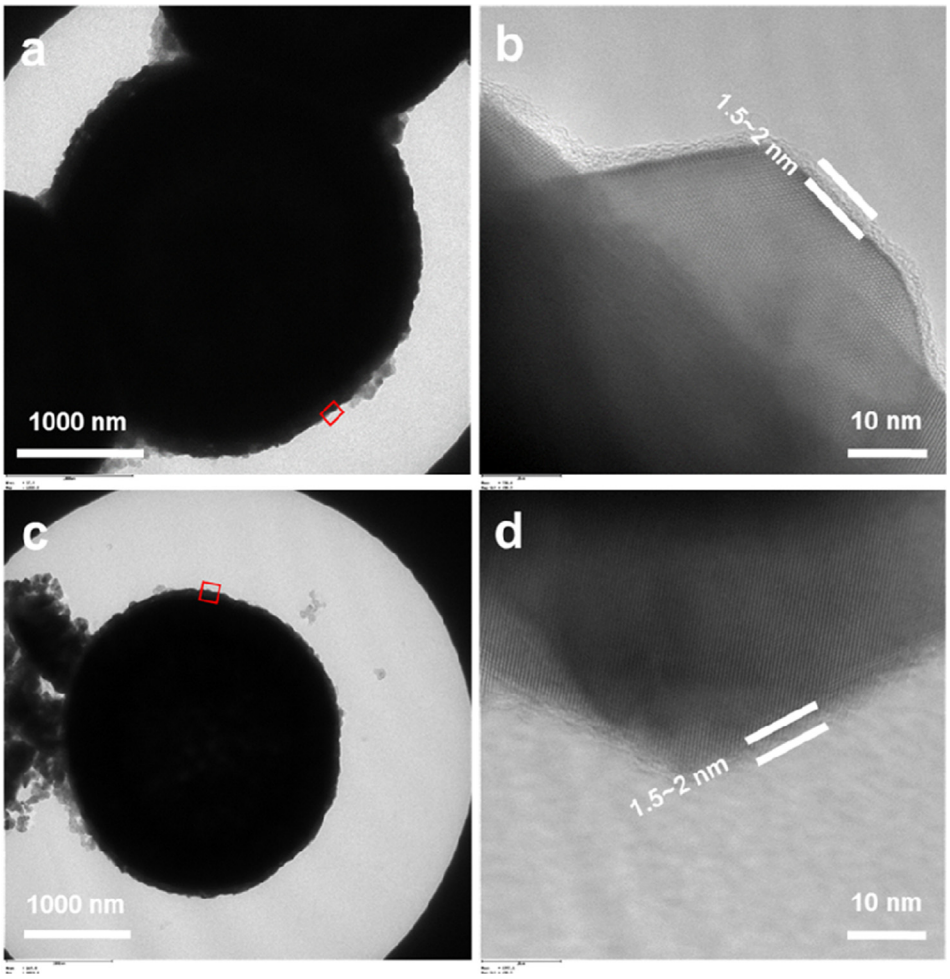

Fig. 8. TEM (a, c) and HRTEM (b, d) images of the LNMO1 (a, b) and LNMO2 (c, d) after 5 cycles.

surfaces of both the samples after cycle. Such layers with certain thickness are believed to have interaction with the pores involved in the two microspheres. According to the previous BJH pore size distribution curves, LNMO1 has concentrated pores diameter around 2.2 nm, in contrast, LNMO2 is equipped with most pores larger than 3.5 nm. As schematically illustrated in Fig. 9, tinier pores in LNMO1 are supposed to be easily shut down and filled with the undesired substance after the deposition of SEI layer, hence it leads to decrease of active sites and the consistency of the cathode material. While its counterpart with large pores beyond the diameter of double SEI layer is suggested to be preferably less influenced by that.

Besides, the pore conditions of LNMO1 and LNMO2 are closely correlated with their surface area according to the BET measurements. Moreover, the tap density tests of the two materials show that densities of them are respectively 1.07 g mL^{-1} (LNMO1, $V = \sim 4.5$ mL, $m = 4.805$ g) and 1.08 g mL^{-1} (LNMO2, $V = \sim 4.5$ mL, $m = 4.853$ g), and the similarity of their tap density mirrors that the mass of single microspheres in the two products are approximately the same, hence the pore volumes of them in microspheres are similar as well. As a result, the correlation between the pore condition and surface area is credible that microspheres with tinier pores have higher surface area while the ones with larger pores are on the contrary. Since it is established that high surface area increases the incidence of undesirable electrode/electrolyte reactions thereby resulting in poorer performance [11,12,20]. The LNMO1 with tinier pores and higher surface area corresponds to poorer performance, while the LNMO2 on the contrary is able to realize reasonable performance.

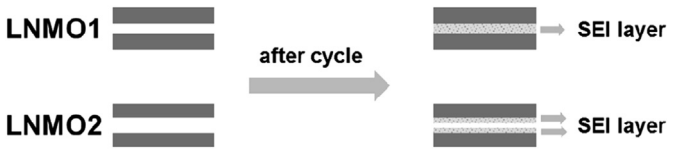

Fig. 9. Schematic illustration of the variation of pores conditions before and after cycle.

As discussed above, the two explanations can correlated with each other by the pore condition of the LNMO microspheres: tinier pores suffer from adverse change due to their parameter, additionally, the corresponding large surface area increases the hazard of undesirable electrode/electrolyte reactions as well. In comparison, LNMO2 porous microspheres with larger and less pores here convincingly exhibit excellent performance that indicates the merits of such nanostructures as well as the intrinsic properties of LNMO. By comparing the two types of $LiNi_{0.5}Mn_{1.5}O_4$ microspheres with different pore conditions and their electrochemical performance, it is convincing that the strategy to boost the performance of electrode materials by nanostructuring requires more modifications rather than being simply excluded. And more in-depth mechanism behind the influence of pore parameters coupled with surface area towards electrochemical performance is necessarily an area of future investigation.

4. Conclusions

In summary, in this paper we introduce a facile approach to preparing two types of LNMO microspheres with different pore condition by switching two kinds of lithium resources: LiOH or Li_2CO_3. As cathodes materials in LIBs, they show distinct electrochemical performance, especially under higher discharge rate. Specifically, LNMO microspheres with larger pores exhibit much more excellent performance compared with their counterparts on the opposite. Such difference is discussed to be derived from two aspects, as one of the proposed explanations, the larger pores are supposed to be less influenced by the deposition of SEI layer, another reason is that LNMO microspheres with large pores have lower specific surface area which favors its performance.

Acknowledgments

This work was supported by the 973 Project of China (No. 2011CB935901), the National Natural Science Fund of China (No. 91022033, 21201158), Anhui Provincial Natural Science Foundation (1208085QE101).

References

[1] Q.M. Zhong, A. Bonakdarpour, M.J. Zhang, Y. Gao, J.R. Dahn, J. Electrochem. Soc. 144 (1997) 205–213.
[2] S. Patoux, L. Daniel, C. Bourbon, H. Lignier, C. Pagano, F. Le Cras, S. Jouanneau, S. Martinet, J. Power Sources 189 (2009) 344–352.
[3] R. Santhanam, B. Rambabu, J. Power Sources 195 (2010) 5442–5451.
[4] A.S. Arico, P. Bruce, B. Scrosati, J.M. Tarascon, W. Van Schalkwijk, Nat. Mater. 4 (2005) 366–377.
[5] H. Xia, Y.S. Meng, L. Lu, G. Ceder, J. Electrochem. Soc. 154 (2007) A737–A743.
[6] J. Yang, X. Han, X. Zhang, F. Cheng, J. Chen, Nano Res. 6 (2013) 679–687.
[7] H.-W. Lee, P. Muralidharan, C.M. Mari, R. Ruffo, D.K. Kim, J. Power Sources 196 (2011) 10712–10716.
[8] X. Zhang, F. Cheng, K. Zhang, Y. Liang, S. Yang, J. Liang, J. Chen, RSC Adv. 2 (2012) 5669–5675.
[9] X. Zhang, F. Cheng, J. Yang, J. Chen, Nano Lett. 13 (2013) 2822–2825.
[10] L. Zhou, D. Zhao, X. Lou, Angew. Chem. Int. Ed. 51 (2012) 239–241.
[11] Y. Talyosef, B. Markovsky, R. Lavi, G. Salitra, D. Aurbach, D. Kovacheva, M. Gorova, E. Zhecheva, R. Stoyanova, J. Electrochem. Soc. 154 (2007) A682–A691.
[12] J. Cabana, M. Casas-Cabanas, F.O. Omenya, N.A. Chernova, D. Zeng, M.S. Whittingham, C.P. Grey, Chem. Mater. A Publ. Am. Chem. Soc. 24 (2012) 2952–2964.
[13] X. Chen, K. Sun, E. Zhang, N. Zhang, RSC Adv. 3 (2013) 432–437.
[14] J.R. Ying, C.Y. Jiang, C.R. Wan, J. Power Sources 129 (2004) 264–269.
[15] X. Xiao, J. Lu, Y. Li, Nano Res. 3 (2010) 733–737.
[16] M.-Y. Cho, K.-B. Kim, J.-W. Lee, H. Kim, H. Kim, K. Kang, K.C. Roh, RSC Adv. 3 (2013) 3421–3427.
[17] L. Shen, C. Yuan, H. Luo, X. Zhang, K. Xu, Y. Xia, J. Mater. Chem. 20 (2010) 6998.
[18] H.-B. Kang, S.-T. Myung, K. Amine, S.-M. Lee, Y.-K. Sun, J. Power Sources 195 (2010) 2023.
[19] H. Wu, I. Belharouak, A. Abouimrane, Y. Sun, K. Amine, J. Power Sources 195 (2010) 2909.
[20] M. Ma, B. Kang, R. Lavi, G. Ceder, J. Electrochem. Soc. 157 (2010) A925–A931.